Research article

Journal of RAMAN SPECTROSCOPY

Received: 2 January 2014 Revised: 16 May 2014 Accepted: 2 June 2014 Published online in Wiley Online Library

(wileyonlinelibrary.com) DOI 10.1002/jrs.4532

Raman investigation of artificial patinas on recent bronze protected by different azole type inhibitors in an outdoor environment†

Tadeja Kosec,[a]* Andraž Legat[a] and Polonca Ropret[b,c]

Bronze surfaces, as well as prepatinated surfaces on bronze, undergo chemical and visual changes when exposed to humid and polluted environments. For this reason, it is important to study the effectiveness of corrosion inhibitors on patinated-bronze surfaces. The aim of this study was to investigate different protection systems for patinated bronze, which are based on the use of two azole type inhibitors: 2-mercaptobenzimidazole and benzotriazole. The results of our practice confirmed that these inhibitors were very effective when immersed in a corrosive solution containing inhibitor for 24 h. The inhibited layers were then protected by a water-repellant layer. In the case of the studied patinas, green chloride and green nitrate patinas, applied over the brown artist's patina, were tested, as well as brown patina and the patina that develops on bare bronze. The study was performed after each chemical patination and the application of the two different inhibitors.

The inhibition systems used on the different chemically achieved patinas were characterized by Raman spectroscopy and electrochemical techniques. The results of the Raman studies showed a chemical interaction of both inhibitors with copper and bronze but a versatile interaction between the inhibitors and the different patinas. The chemical interaction of benzotriazole was observed on the nitrate patina, whereas the mercaptobenzimidazole showed interaction also with the chloride-type patina. Electrochemical tests proved the interaction, which had been detected by Raman spectroscopy.

Keywords: bronze; artist's patina; corrosion inhibitors; Raman spectroscopy; linear polarization

Introduction

Bronze is widely used for sculptures and other art objects. These objects are usually covered by a layer of patina. These layers can either be formed spontaneously during years of exposure or they can be artificially applied by using various solutions of inorganic salts. The acid rain, which is the result of the presence of polluting gasses, can cause extensive damage to bronze objects and patina layers. SO_2 and NO_x are the main pollutants in urban atmosphere, due to the industrial activity and traffic emissions.[1] The origin of patinas and the degraded state of bronze works of art are also both important for the planning of the proper conservation treatment for such objects, as well as for the establishing of environmental conditions, which are suitable for their storage and display. In the authors' previous work, it was shown that it is possible, by means of Raman spectroscopy, to differentiate between artists' applied patinas and patinas, which have been formed because of environmental exposure.[2] It is usually expected that both bronze and its patinas will be preserved because of their artistic and archeological value. In order to satisfy the requirements for cultural heritage objects (e.g., an unaltered appearance or a removable protective system), only certain corrosion protection methods may be used. Some common methods used as protective systems by conservators are waxes, varnishes and lacquers, and corrosion inhibitors. Often, a combination of these protection systems is applied.[3–6]

The use of corrosion inhibitors is one of the methods for protecting patinas. Because the inhibitors used for protection are often toxic (i.e. benzotriazole (BTA)), new non-toxic inhibitors are now being developed and tested.[7–15] BTA is the most common corrosion inhibitor for bronze in the conservation field. It is well known that its high inhibition efficiency is achieved on bare copper and copper alloys, but its efficiency on patinated copper surfaces is limited. Electrochemical patina formed on bronze was most protected by BTA when compared with aminotriazole and bitriazole.[7] In the case of electrochemical patinas, it has been shown that imidazole-type inhibitors can be equally efficient as BTA.[15] However, only a few studies have been performed on chemical patinations.[7,12,15,16] It is important to obtain information about the inhibition efficiency of those inhibitors, which are most often applied to chemical patinas. Because BTA is now being abandoned, because of its toxicity, new inhibitors have been investigated, such as imidazole-type inhibitors. The adsorption orientation and characterization of 2-mercaptobenzimidazole (MBI) has been studied on an Au(111)

* *Correspondence to: Tadeja Kosec, Slovenian National Building and Civil Engineering Institute, Dimičeva 12, SI-1000 Ljubljana. E-mail: tadeja.kosec@zag.si*

† *This article is part of the special issue of the Journal of Raman Spectroscopy entitled "Raman in Art and Archaeology 2013" edited by Polonca Ropret and Juan Manuel Madariaga.*

a *National Building and Civil Engineering Institute, Dimičeva 12, 1000 Ljubljana, Slovenia*

b *Conservation Centre, Institute for the Protection of the Cultural Heritage of Slovenia, Poljanska 40, 1000 Ljubljana, Slovenia*

c *Museum Conservation Institute, Smithsonian Institution, 4210 Silver Hill Rd., Suitland, MD 20746*

electrode, both electrochemically and spectroscopically.[17–20] However, the application of MBI to copper, bronze, and patinated bronze has not yet been studied. Apart from the fact that imidazole inhibitors are environmentally friendly,[9] they have been found to exhibit a high-inhibiting efficiency in the protection of copper in sulfuric acid[9,10] and in near neutral chloride solutions.[11] The results of previous studies have also shown that some imidazole derivatives can provide efficient long-term protection to patinated bronze in simulated acid rain.[12,13] Other environmentally friendly compounds, such as the 4-methyl-1-(*p*-tolyl)-imidazole inhibitor, have proved to be good corrosion inhibitors for copper and its alloys in various aggressive environments.[15,16]

In this work, the protective effect of the two azole-based corrosion inhibitors, used alone or in combination with carnauba wax to form the final protection of the chosen patinas on bronze, was studied by electrochemical and Raman investigation. BTA, which is traditionally used in conservation practice, was compared with 2-MBI, a compound known as a by-product in the pharmaceutical industry. The increased inhibition efficiency of inhibitors on patinated bronzes, achieved by electrochemistry, can be explained by interactions and studied by Raman spectroscopy.

The efficiency of protection systems can be validated by monitoring their stability and degree of protection provided when exposed to corrosive media. In this work, the protective effect of corrosion inhibitors and carnauba waxes was examined in the laboratory by means of electrochemical methods.

For this purpose, three chemical patinas were tested: a brown sulfide-type patina, a green chloride patina, and a green nitrate patina. Each of them was treated with the two inhibitors by immersion in a corrosive solution, which was proved to be the most efficient way of applying the inhibitors to the patinas.[16] The action of the inhibitors was studied by electrochemical methods in order to define their corrosion inhibition efficiency and by Raman analysis in order to study the type of bonding between the two inhibitors (BTA and 2-MBI) and the patinated and non-patinated-bronze surfaces.

Experimental

Sample preparation

The bronze samples were casted at a foundry and consisted of 87 (w) % copper, 5.5 (w) % tin, 3.2% of zinc, 0.6% of Al, and 3.2% of the impurities as analyzed by an X-Ray Flourescence (XRF) Analyser (spectra not shown). Samples for the electrochemical tests and the Raman analysis were cut from the plates and abraded with 800-grid and 1000-grid SiC paper. The samples were cleaned in acetone and then dried in air flow.

As mentioned earlier, three different patinas were studied: a brown patina, a green chloride patina, and a green nitrate patina. First, a brown patina was achieved on the bronze by brushing the hot surface with a 3% solution of K_2S. Green patinas were grown over the brown patina. A chloride-type green patina was produced over the warm surface by brushing with a solution of ammonium carbonate and ammonium chloride (30 g/l each). The nitrate patina was achieved by brushing the hot brown bronze surface with a 3% solution of $Cu(NO_3)_2$.

The following finishes were tested: a 3% solution of 2-MBI and BTA in an ethanol solution applied by a brushing technique, a 3% solution of both inhibitors in a corrosive solution of acid rain applied by 24-h immersion, and a protection system consisting of the inhibited surface with hydrophobic Carnauba wax as the final coating. Carnauba wax was melted in white spirit and applied over the bronze surfaces using a brush. The structures of both inhibitors are presented in Fig. 1.

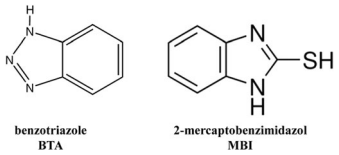

Figure 1. The tested inhibitors: (a) benzotriazole and (b) 2-mercaptobenzimidazole.

Exposures and testing conditions

The electrochemical tests of the patinas and the different protection systems were tested in a solution of 0.2 g l^{-1} Na_2SO_4, 0.2 g l^{-1} $NaHCO_3$, and 0.2 g l^{-1} $NaNO_3$ (simulated acid rain), which was acidified to pH 5 with diluted H_2SO_4 in order to simulate urban rain. A three-electrode corrosion cell was used, with a volume of 350 cm^3. The working electrode was embedded in a Teflon holder and had an exposed area of 0.785 cm^2. Autolab PGStat 100, Floating version equipment operated by Nova software 1.8 was used.

The electrochemical tests were performed as follows: 2-h stabilization at open circuit potential (OCP), with linear polarization measurements at ± 20 mV *versus* OCP at a scan rate of 0.1 mV/s. The potentiodynamic measurements were then performed starting from −0.25 V *versus* OCP, and progressing in the anodic direction up to +2.0 V at a scan rate of 1 mV/s. All the potentials are reported with respect to the SCE scale.

Raman spectroscopy

The Raman spectra of the investigated patinas and inhibitor systems were recorded using 632-nm and 514-nm laser excitation lines with a Horiba Jobin Yvon LabRAM HR800 Raman spectrometer (Horiba Yvon, France, 2008), coupled with an Olympus BXFM optical microscope (Olympus, UK, 2008). The spectra were recorded using a 100× objective lens and 600 grooves/mm grating, which gave a spectral resolution of cca. 1 cm^{-1}/pixel. The power used in these tests was set between 0.1 and 0.6 mW using neutral density filters. A multi-channel, air-cooled CCD detector was used, with integration times of between 20 and 35 s, and the spectral range was set to between 50 and 4000 cm^{-1}. The wave number calibration was performed using a silicon wafer. The spectra are presented with no baseline correction.

Results and discussion

Raman investigation of benzotriazole and 2-MBI bonding on copper and bronze

Raman results on BTA and 2-MBI applied to bare copper, bronze, and different artificial patinas are presented in Figs. 2–5. In the previous studies,[21] it was demonstrated that BTA shows bonding to bare copper through a triazole ring, as a shift of the Raman modes assigned to triazole ring breathing and stretching occurs. In the present study, bands of crystalline BTA corresponding to triazole ring breathing occurred at 1130 and 1212 cm^{-1} [Fig. 2(a)], and the triazole ring stretching at 1390 cm^{-1} is shifted to cca. 1152 and 1194 cm^{-1} and to 1395 cm^{-1} [Fig. 2(b)], respectively, when BTA is applied to bare copper. It is difficult to assign exact positions to the bands belonging to triazole ring breathing because the bands appear to be very weak and are obscured by

Journal of RAMAN SPECTROSCOPY

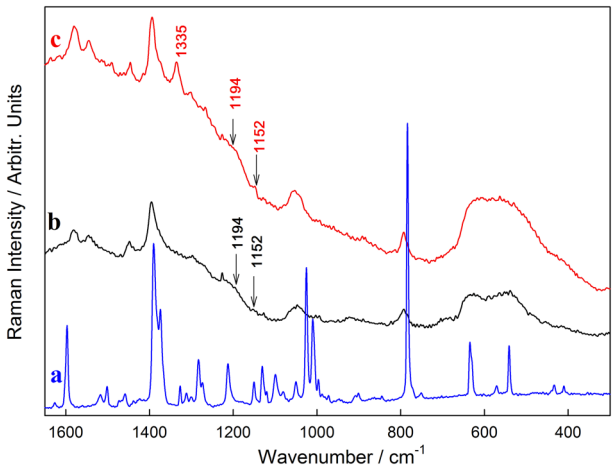

Figure 2. Raman spectra (excitation line 632 nm) of benzotriazole film on copper and bronze after immersion in a 3% BTA solution in simulated acid rain: (a) crystalline BTA, (b) BTA applied on copper, and (c) BTA applied on bronze.

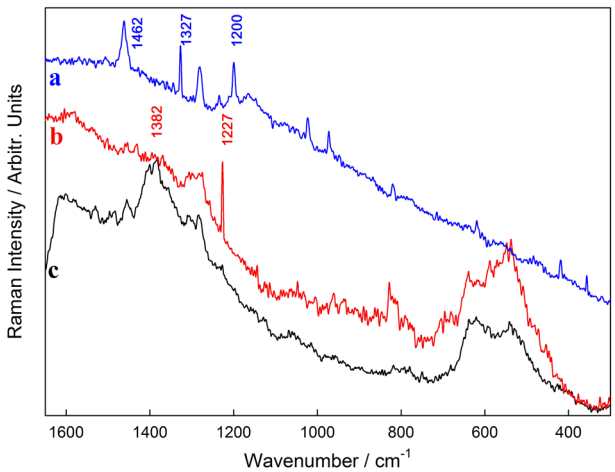

Figure 3. Raman spectra (excitation line 632 nm) of MBI bonding on copper and bronze after immersion in a 3% MBI solution in simulated acid rain: (a) crystalline MBI, (b) MBI applied on copper, (c) MBI applied on bronze.

the fluorescent background. The authors' previous studies using X-ray photoelectron spectroscopy showed that there is a chemical bonding between the BTA and the copper (I), as observed from the chemical shift, i.e. Cu_2O can be detected from the Cu LMM spectra at E_b 569.9 eV and Cu(I)BTA at E_b 572.6 eV,[8] which is a clear evidence that, as an inhibitor, BTA forms a chemical bond with Cu_2O.[8] In the Raman spectrum of BTA applied on bare copper, also, the formation of copper oxides can be detected through the broadened band in the region between 700 and 400 cm^{-1} [Fig. 2(b)]. The formation of oxides is expected as a weak acid solution that was used during the BTA application. Similar results of copper bonding to BTA were also obtained when BTA was applied on bronze [Fig. 2(c)], as bands at 1580, 1545, 1447, 1395, 1300, 1225, 1194, 1152, 1050, and 792 cm^{-1} appear at the same wavenumbers and are of the same intensity. This proves that BTA effectively inhibits bare bronze, too. Furthermore, the appearance of a new Raman mode at 1335 cm^{-1} suggests the possible bonding of triazole also to another alloying element present in the bronze, i.e. Sn. Similarly, as in the case of bare copper, the

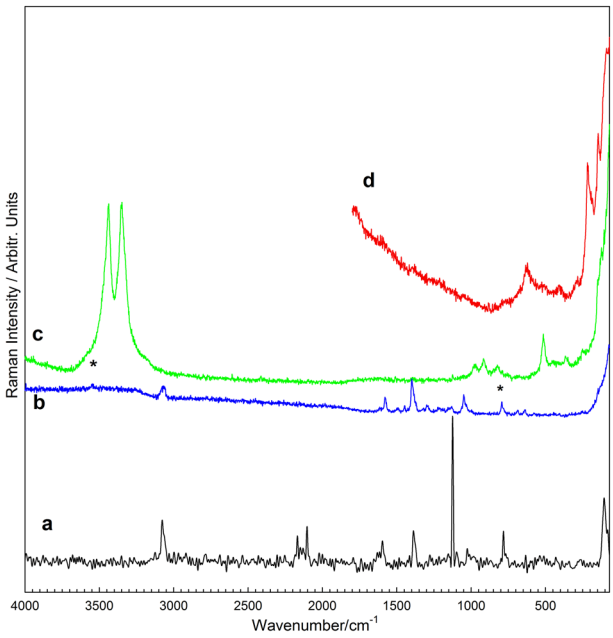

Figure 4. Raman spectra (excitation line 514 nm) of benzotriazole film on different patinas after immersion in a 3% BTA solution in simulated acid rain: (a) crystalline BTA (baseline corrected), (b) BTA applied to nitrate patina, with * marking the bands of nitrate patina, (c) BTA applied to chloride patina, and (d) BTA applied to sulfide patina.

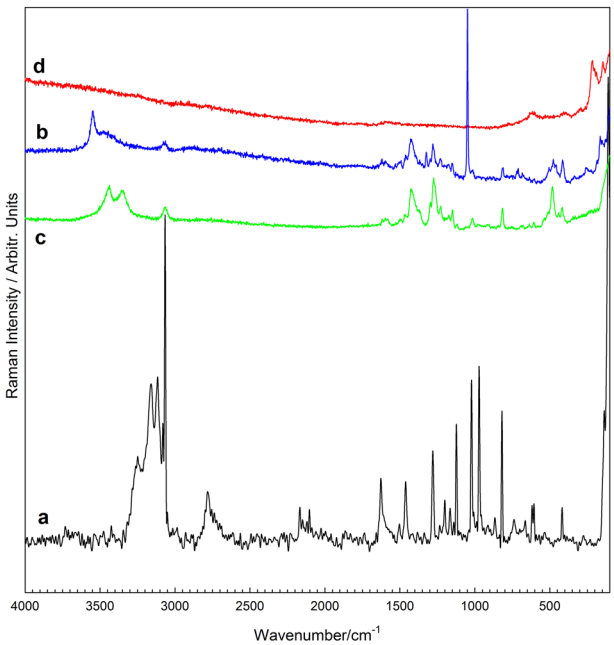

Figure 5. Raman spectra (excitation line 514 nm) of MBI bonding to different patinas after immersion in a 3% MBI solution in simulated acid rain: (a) crystalline MBI (baseline corrected), (b) MBI applied to nitrate patina, (c) MBI applied to chloride patina, and (d) MBI applied to sulfide patina.

broadened band at 700–400 cm^{-1} suggests the presence of copper and tin oxides.

Figure 3 shows the Raman results for the application of 2-MBI to bare copper and bronze using 633-nm excitation. The Raman modes for crystalline MBI appear at 1682, 1462, 1327, 1281, 1234, 1200, 1165, 1123, 1022, 972, 820, 620, 420, and 356 cm^{-1} [Fig. 3(a)]. MBI interaction with gold has been studied by Density

Functional Theory, Fourier Transform Infrared Spectroscopy (FTIR), and Fourier Transform (FT)-Raman measurements.[17–19] On the basis of the published data, the following assignments are possible when using 633-nm excitation. The very weak band at 1682 cm^{-1} can be assigned to aromatic stretch (ν(CC)) and the mode at 1462 cm^{-1} to a contribution of ν(CC) + ν(CN) + δ(NH). C–N stretching is also involved in the 1281 mode, whereas the N–H in-plane antisymmetric bending makes a big contribution to the band at 1234 cm^{-1}. Raman modes involving the CS bond are visible at 1327 cm^{-1} (SCN angular deformations – β(SCN)), 1200 cm^{-1} (ν(CS) + β(NCN) + δ(NH), and the band at 420 cm^{-1} can be assigned to C S stretching (ν(CS)). The presence of the bands (1200 and 420 cm^{-1}) involving C S stretching suggests a rather thione tautomeric form of the MBI.[17,22] Further, very weak bands at 1165, 1123, and 1022 cm^{-1} can be assigned to CH bending (δ(CH)).

When MBI is applied to bare copper, bands can be noticed at 1615, 1455, 1401, 1382, 1354, 1307, 1282, 1227, and 818 cm^{-1} [Fig. 3(b)]. The mode at 420 cm^{-1} (C S stretch) is not visible, and also, the two other bands involving CS at 1327 and 1200 cm^{-1} are shifted to 1307 and 1227 cm^{-1}, respectively. This suggests the bonding of Cu to MBI through S, similarly as was found in the case of MBI bonding to Au.[17] The bands involving (δ(CH)) are not visible, and further shifts are noticeable for the bands at 1682 and 1462 cm^{-1} to 1615 and 1455 cm^{-1}, respectively. According to the study of MBI bonding to Au,[17] this can be explained by the increased aromatic character due to deprotonation.

In the case of MBI application to bronze, the Raman modes appear at 1455, 1432, 1382, 1303, 1282, 1227, and 818 cm^{-1} [Fig. 3(c)]. Again, the band at 420 cm^{-1} (C S stretch) is not visible, and the two other bands involving CS are shifted to 1303 and 1227 cm^{-1}, suggesting the bonding of MBI to bronze through S substituted to the imidazole ring. As in the case of bare copper, a similar shift can be noticed for the ν(CC) + ν(CN) + δ(NH) mode, which can be found at 1455 cm^{-1}.

In both cases, i.e. for pure copper and bronze, broadened bands are seen in the region between 700 and 400 cm^{-1}[Fig. 3 (b,c)] and can be explained by the formation of copper and tin oxides as a weak acid solution was used during the MBI application.

In the case of the investigation of the interaction of the two inhibitors, BTA and MBI with patinas, the 514-nm excitation was used, as no useful data for patinas could be obtained with the 633-nm line. The interaction of BTA with different bronze patinas, such as nitrate, chloride, and sulfide, is shown in Fig. 4, and the bands are presented in Table 1. The bonding of copper to the triazole ring can be found only in the case of the copper nitrate patina [Fig. 4(b)], as the band of triazole ring breathing at 1125 cm^{-1} [Fig. 4(a)] can be noticed at higher wavenumbers, at 1135 cm^{-1}, with a significant loss of intensity, in the case of the BTA applied to the nitrate patina [Fig. 4(b)]. The shift to higher wavenumbers can be noticed also in the case of triazole ring stretching, from 1387 to 1398 cm^{-1}, for the BTA and for the BTA applied to the nitrate patina, respectively. There are only two bands in the spectrum of the BTA applied to the nitrate patina that could be assigned to the patina: the very weak mode at 3548 cm^{-1} and the medium intensity band at 1049 cm^{-1} [Fig. 4(b)]. The latter is usually the strongest band of the nitrate patina belonging to the NO_3 symmetric stretching. The chloride and sulfide patina on the bronze did not show any chemical interaction with the BTA in the Raman spectra [see Fig. 4(c,d)]. In the Raman spectrum of the BTA applied to the chloride patina [Fig. 4(c)], only the bands significant for the patina can be noticed at 3438, 3350, 1126, 975, 913, 823, 516, and 366 cm^{-1}, belonging to atacamite ($Cu_2(OH)_3Cl$),[23,24] a very often found compound of copper and bronze corrosion, when treated with chlorides.[23] Similarly, in the spectrum of BTA applied to the sulfide patina [Fig. 4(d)], only the bands arising from the patina could be noticed. The broader band, with several maxima in the region between 350 and 700 cm^{-1}, suggests the presence of Cu and Sn oxides, whereas the well-defined bands at 218 and 146 cm^{-1} suggest the presence of cuprite.[23,25,26] The weak band at 289 cm^{-1} could also indicate the presence of Cu_2S.[27]

Table 1. The Raman shifts in cm^{-1}

BTA powder	BTA applied on the nitrate patina	BTA applied on the chloride patina	BTA applied on the sulfide patina
	3548[a] vw	3448[a] s	
3078 w	3069 w	3350[a] s	
1595 w	1580 m-w		
	1495 vw		
	1449 vw		
1387 m-w	1398 s-m		
	1299 w		
	1223 vw		
1125 vs	1135 w	1126[a] vw	
	1049[a] m		
1027 vw	1030 wsh	975[a] vw	Broadened
1009 vw	1001 vw	913[a] w	band
			350–700[a]
783 w	795 w	823[a] vw	289[a] vw
	687 vw	516[a] m-w	218[a] m
	641 vw	366[a] vw	146[a] m

BTA, benzotriazole.
The relative intensities measured on reference BTA powder and BTA applied on the nitrate, chloride, and sulfide patina are given as follows: (vs) very strong, (s) strong, (m) medium, (w) weak, (vw) very weak, and (sh) shoulder.
[a]Belong to patinas only.

The results of the application of MBI to the selected bronze patinas are shown in Fig. 5, and the observed bands are listed in Table 2. Using 514-nm excitation, the Raman modes of MBI at 3300–3000 cm^{-1} also became visible [Fig. 5(a)]. The bands at 3249 and 3159 cm^{-1} can be assigned to N–H stretching and those at 3115, 3080, and 3065 cm^{-1} to C–H stretching.[17] Most of the other bands described earlier in the text appear at the same wavenumbers as for the MBI recorded with 633-nm excitation. One of the very weak bands assigned to the aromatic stretch (ν(CC)) at 1682 cm^{-1} is not visible, but the band, also assigned to (ν(CC)), appears weak at 1627 cm^{-1}. Furthermore, the mode at 1327 cm^{-1}, assigned to SCN angular deformations, is not visible, whereas bands at 1200 (ν(CS) + β(NCN) + δ(NH) and 419 cm^{-1} (ν(CS)) can be clearly detected. Additionally, the thione tautomeric form of pure MBI is indicated by the absence of the band significant for S–H stretch that can be expected for the aromatic thiols in the 2600–2500 cm^{-1} range.[22] When MBI is applied to the chloride [Fig. 5(b)] and nitrate [Fig. 5(c)] patina, the weak bands of patinas in the 500–400 cm^{-1} spectral range (see Fig. 5 and Table 2) overlap with the range where (ν(CS)) is expected. For this reason, the 419 cm^{-1} band of pure MBI cannot be used for the evaluation of the MBI bonding to Cu through S

Journal of RAMAN SPECTROSCOPY

Table 2. The Raman shifts in cm^{-1}

MBI powder	MBI applied on the nitrate patina	MBI applied on the chloride patina	MBI applied on the sulfide patina
	3550[a] m	3438[a] m	
	3472[a] (m-w)br	3350[a] m	
3249 m-w			
3159 m			
3115 m			
3080 m-w	3076 vw	3082 wsh	
3065 s	3063 vw	3065 w	
1627 w	1620 vw	1620 vw	
		1580 vw	
		1497 vw	
1462 w	1460 w	1458 w	
	1425 m-w	1427 m	
	1394 wsh	1370 wsh	
		1297 m-w	
	1324[a] w		
1280 m-w	1280 m-w	1275 m	
1234 vw	1234 vw		
1200 w	1225 vw	1227 m-w	
1166 w	1150 vw	1150 m-w	
1124 m		1117 vw	
1023 s-m	1049[a] vs	1016 vw	
972 s-m		980[a] vw	
		970[a] vw	
		910[a] vw	
819 m	815[a] vw	816[a] m-w	
737 vw			
	713[a] vw		
665 vw		678 vw	Broadened band 700–350[a]
618 vw			
605 vw		608 vw	
	507[a] w	514[a] wsh	
	475[a] w	483 m	
	456[a] w		
		441[a] w	
419 vw	416[a] w	417[a] w	
		355[a] vw	
	259[a] vw		290[a] vw
			217[a] m
			146[a] m

MBI, mercaptobenzimidazole.
The relative intensities measured on reference MBI powder and MBI applied on the nitrate, chloride, and sulfide patina are given as follows: (vs) very strong, (s) strong, (m) medium, (w) weak, (vw) very weak, and (sh) shoulder.
[a]Belong to patinas only.

substituted to the imidazole ring. The only useful information regarding the Cu–S bonding can be obtained with the shift of the 1200 cm^{-1} mode to 1227 cm^{-1} in the case of the chloride patina and to 1225 cm^{-1} in the case of the nitrate patina. Interestingly, also, the 3300–3000 cm^{-1} spectral range of MBI, when it is applied to both, i.e. the chloride and nitrate patinas [Figs. 5(b,c)), is strongly affected, as only very weak modes significant for the CH stretch can be found at 3082, 3063 cm^{-1} and at 3076, 3063 cm^{-1}, respectively. This could be further the proof of the deprotonation of MBI upon reaction with copper or it could be ascribed to copper bonding also to N in the imidazole ring. Further research is needed to obtain an answer to this question.

In addition to the evidence of the MBI bonding to the chloride and nitrate patinas, bands which are significant for atacamite [Fig. 5(b)] and gerhardite [Fig. 5(c)], respectively, can also be found. The bands of atacamite[23,24] appear at 3438, 3350, 980, 970, 910, 816, 678, 514, 441, 417, and 355 cm^{-1}, whereas modes of gerhardite[23,24] ($Cu_2(OH)_3NO_3$) can be found at 3550, 3472, 1324, 1049, 815, 713, 507, 475, 456, 416, and 259 cm^{-1}.

The sulfide patina [Fig. 5(d)], again, did not show any interaction with the inhibitor, in this case MBI. Similar to the BTA results, only Cu and Sn oxides, cuprite, and the possible presence of Cu_2S could be detected [Fig. 5(d)].

Electrochemical testing of the different protection systems

In order to determine the inhibition efficiency of the different protection systems on the patinas, electrochemical test were performed.

The electrochemical data of the sulfide patina, treated with different inhibition systems, are presented in Table 1 and in Fig. 6. It can be observed from the measured electrochemical parameters that brushing the sulfide patina with ethanol solutions of the inhibitors only slightly increases the polarization resistance of the sulfide patina, brushed with BTA (3.2 $k\Omega \cdot cm^2$ in comparison with 2.1 $k\Omega \cdot cm^2$ for the sulfide patina, respectively). Treating the sulfide patina in an acid solutions containing inhibitor for 24 h increased the polarization resistances of such treated surfaces by a factor of 22.9 in the case of MBI and 8 in the case of BTA, whereas the highest polarization resistances are achieved when the inhibition system was protected by an additional layer of carnauba wax. From the data given in Table 3, it can be concluded that the wax provides very good protection for the under-layer surface, as was observed in previous studies.[16]

The electrochemical data of the nitrate patina, treated with different inhibition systems, are presented in Table 4 and in Fig. 7. The corrosion current density of the nitrate patina (23 $\mu A\,cm^{-2}$) was higher than that of the sulfide patina (12 $\mu A\,cm^{-2}$), indicating that in simulated acid rain, the nitrate patina is more reactive.

Brushing the patina with an ethanol solution of the inhibitors did not increase the polarization resistance of the treated surfaces, whereas 24-h immersion in an inhibitor containing an acid solution increased the polarization resistance of the nitrate patina treated in BTA by a factor of 2.4 and that treated by MBI for a factor of 5. An additional layer of Carnauba wax provides good corrosion resistance, based on the high measured values of polarization resistances (Table 4), as already observed in the case of the sulfide patina.

The electrochemical data of the chloride patina, treated with different inhibition systems, are presented in Table 5 and Fig. 8. The chloride patina appears to be very unstable, brushing the green chloride patina with an ethanol solution of the inhibitor did not change its polarization resistance value. Furthermore, the same observation can be made in the case when the patina was treated for 24 h in an acid solution of BTA. Thus, it was found that polarization resistance increases by a factor of 12 in the case of a chloride patina treated with 2-MBI. It can be concluded, as an inhibitor, that BTA is not effective for chloride-type patinas, whereas 2-MBI improves the stability of chloride patina.

Table 3. The electrochemical parameters deduced from the linear polarization measurements for the sulfide patina

	E_{corr} [mV]	j_{corr} [$\mu A\,cm^{-2}$]	R_p [$k\Omega\,cm^2$]
Sulfide	−74	12.5	2.1
Sulfide + BTA	−41	8.1	3.2
Sulfide + BTA 24 h	−23	1.5	16.9
Sulfide + BTA 24 h + carnauba	10.8	0.003	9120
Sulfide	−74	12.5	2.1
Sulfide + MBI	−27	13.5	1.9
Sulfide + MBI 24 h	35	0.54	48
Sulfide + MBI 24 h + carnauba	−132	0.041	631

Table 4. The electrochemical parameters deduced from the linear polarization measurements for the nitrate patina

	E_{corr} [mV]	j_{corr} [$\mu A\,cm^{-2}$]	R_p [$k\Omega\,cm^2$]
Nitrate patina	87	23	1.1
Nitrate + BTA/EtOH	108	19	1.4
Nitrate + BTA 24 h	102	9.9	2.6
Nitrate + BTA 24 h + carnauba	163	0.013	1940
Nitrate patina	87	23	1.1
Nitrate + MBI/EtOH	61	17.6	1.48
Nitrate + MBI 24 h	97	4.7	5.57
Nitrate + MBI 24 h + carnauba	170	0.000203	128×10^3

Once again, the additional layer of carnauba wax substantially increased the polarization resistance of the system.

The Raman spectra for chloride patina with BTA and MBI coincide with the fact that chloride-type patina interacts with 2-MBI but not with BTA. The electrochemical results prove that the observation as R_p for 2-MBI is greater than that for BTA (Table 5). Similarly, in the case of nitrate-type patina, the electrochemical results show increased R_p values in the case of nitrate patina in BTA and MBI several fold. Furthermore, indication in the Raman spectra for BTA chemical bonding was proved, as well as for MBI.

However, the investigation of sulfide patina in relation to inhibitors did not give consistent Raman and electrochemical data. The Raman studies did not prove the existence of any molecular bonding of the inhibitors to the patina, whereas the

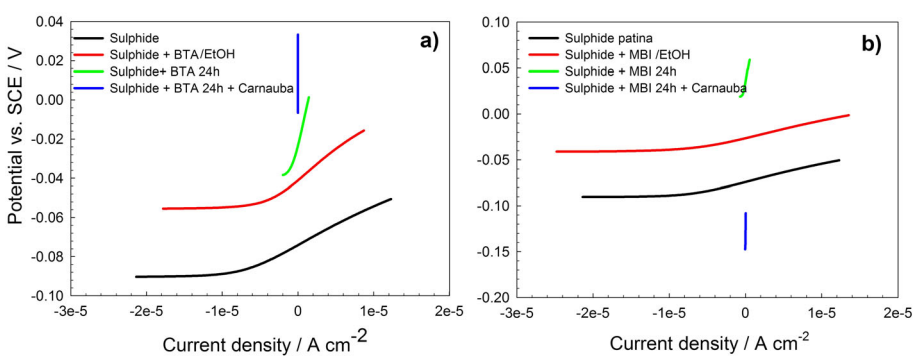

Figure 6. Chloride patina, treated with different protection systems in benzotriazole (BTA), (a) and with 2-mercaptobenzimidazole (MBI), (b). Nitrate patina, treated with different protection systems in benzotriazole (BTA), (a) and with 2-mercaptobenzimidazole (MBI), (b).

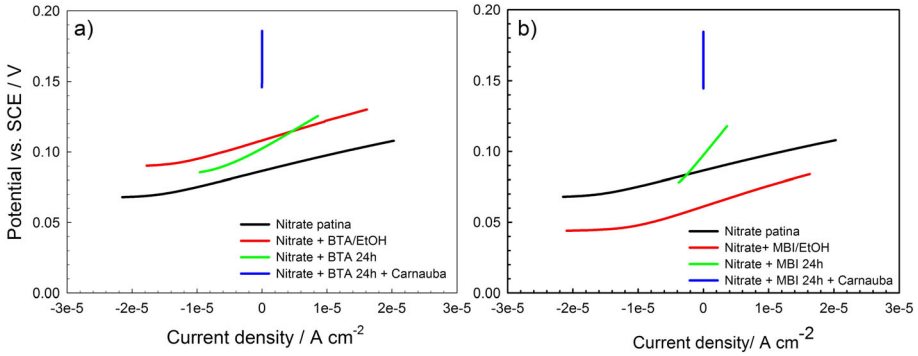

Figure 7. Chloride patina, treated with different protection systems in benzotriazole (BTA), (a) and with 2-mercaptobenzimidazole (MBI), (b).

Table 5. The electrochemical parameters deduced from linear polarization measurements for the chloride patina

	E_{corr} [mV]	j_{corr} [$\mu A cm^{-2}$]	R_p [$k\Omega \cdot cm^2$]
Chloride	−41	22	1.2
Chloride + BTA	160	19	1.4
Chloride + BTA 24 h	−30	28	0.94
Chloride + BTA 24 h + carnauba	−94	0.033	783
Chloride	−41	22	1.2
Chloride + MBI	46	15	1.7
Chloride + MBI 24 h	−11	1.8	14.5
Chloride + MBI 24 h + carnauba	123	0.00007	3.8×10^5

electrochemical results showed an eight-fold increase in the case of BTA and a 22-fold increase in the polarization resistance R_p of the protected sulfide-type patina with MBI. This could be an indication of only physical bonding of inhibitors to the brown patina. Nevertheless, it needs to be taken into account that the chemical bonding might not be Raman active and can therefore not be excluded.

Conclusions

Raman analysis and electrochemical experiments were conducted on different chemically obtained patinas on bronze samples. Different finishes were tested: MBI and BTA inhibitors in a 3% ethanol solution and a 3% solution of BTA and MBI in acid rain after 24-h immersion, and Carnauba wax as a top coat as a typical representative of waxes.

Raman studies of both, BTA and MBI, inhibition systems with bare copper and bronze showed the chemical interaction of both inhibitors with copper and bronze. In the case of BTA, bonding of Cu to triazole ring was confirmed for the bare copper samples, whereas in the case of bronze, an additional bond to an alloying element, probably Sn in addition to Cu, is suggested. MBI showed the interaction through S substituted in the imidazole ring for both samples, pure copper and bronze.

In cases of application of inhibitors to patinated-bronze samples, a chemical interaction, proven by Raman spectroscopy, could be noticed only in the case of the nitrate patina for BTA application, whereas in the case of MBI application, the interaction could be noticed also for the chloride patina. Bonding through S is suggested in the case of both patinas, whereas the bonding through N cannot be excluded. However, further research is needed in order to obtain an answer to this question. The sulfide patina did not show any chemical interaction with any of the studied inhibitors.

The electrochemical results showed that none of the investigated chemically prepared patinas could protect the underlying bronze from further corrosion processes. The inhibitors applied as 3% solution in ethanol do not seem to protect the underlying patinas in the case of all the tested patinas. The protective behavior of MBI and BTA inhibitors after 24-h immersion in acid rain is increased on the nitrate and sulfide patina. The MBI showed better protective properties on the green chloride patina than BTA. Wax is a hydrophobic barrier to the patina and inhibitor system. If it is perfectly applied, it acts as a good barrier against the start of corrosion processes and patina changes.

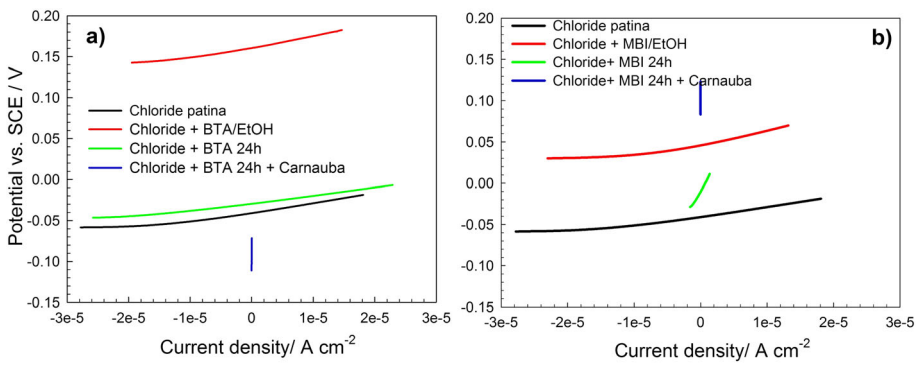

Figure 8. Chloride patina, treated with different protection systems in benzotriazole (BTA), (a) and with 2-mercaptobenzimidazole (MBI), (b).

Acknowledgement

The financial support of the Slovenian Research Agency, grant No. P2-0273 is gratefully acknowledged.

References

[1] R. W. Revie, Uhlig's Corrosion Handbook (3rd edn), John Wiley& Sons: New Jersey, **2011**.
[2] T. Kosec, P. Ropret, A. Legat, *J. Raman Spectrosc.* **2012**, *43*, 1587.
[3] G. Bierwagen, T. J. Shedolsky, K. Stanek, *Prog. Org. Coat.* **2003**, *48*, 289.
[4] V. Argyropouls, E. Angelini, C. Degrigny, Proceedings of Metal 2004, Canberra, Australia, October, **2004**, National Museum of Australia, p.43.
[5] E. Franceschi, P. Letardi, G. Luciano, *J. Cult. Her.* **2006**, *7*, 166.
[6] A. Galtayries, A. Mongiatti, P. Marcus, C. Chiavari, in Corrosion of Metallic Heritage Artefacts, (Eds.: P. Dillmann, *et al.*), EFC Woodhead Publishers, Oxford, **2007**, pp. 335–351.
[7] K. Rahmouni, H. Takeonutti, H. Hajjjaji, A. Srhiri, L. Robbiola, *Electrochim. Acta* **2009**, *54*, 5206.
[8] T. Kosec, D. Kek-Merl, I. Milošev, *Corros. Sci.* **2008**, *50*, 1987.
[9] E. Stupnišek-Lisac, A. Lončarič Božić, I. Cafuk, *Corrosion* **1998**, *54*, 713.
[10] E. Stupnišek-Lisac, A. Gazivoda, M. Mažarac, *Electrochim. Acta* **2002**, *47*, 4189.
[11] H. Otmačić, E. Stupnišek-Lisac, *Electrochim. Acta* **2003**, *48*, 985.
[12] K. Marušić, H. Otmačić-Ćurković, Š. Horvat-Kurbegović, H. Takenouti, E. Stupnišek-Lisac, *Electrochim. Acta* **2009**, *54*, 7106.
[13] L. Muresan, S. Varvara, E. Stupnišek-Lisac, H. Otmačić, K. Marušić, S. Horvat-Kurbegović, L. Robbiola, K. Rahmouni, H. Takenouti, *Electrochim. Acta* **2007**, *52*, 7770.
[14] K. Rahmouni, S. Joiret, L. Robbiola, A. Srhiri, H. Takenouti, V. Vivier, Proceedings of the International Workshop "Advanced Techniques for Energy Sources Investigation and Testing", Sofia, Bulgaria 4 – 9 Sept. **2004**, p8-1–p8-11.
[15] H. Otmačić Ćurković, T. Kosec, A. Legat, *Electrochim. Acta* **2012**, *83*, 28.
[16] T. Kosec, H. Otmačić Ćurković, A. Legat, *Electrochim. Acta* **2010**, *56*, 722.
[17] T. Deneoux, F. Tielens, P. Geerlings, C. Buess-Herman, *J. Phys. Chem. A* **2006**, *110*, 11346.
[18] T. Deneoux, C. Buess-Herman, J. Lipkowski, *J. Electroanal. Chem.* **2004**, *64*, 65.
[19] T. Deneoux, C. Buess-Herman, M. G. Hosseini, R. J. Nichols, J. Lipkowski, *Electrochim. Acta* **2005**, *50*, 4275.
[20] M. G. Hosseini, T. Shahrabi, R. J. Nichols, *Iran. J. Sci. Technol. Trans. A* **2005**, *29*, 49.
[21] M. Metikoš-Huković, R. Babić, A. Marinović, *J. Electrochem. Soc.* **1998**, *145*, 4045.
[22] D. Lin-Vien, N. B. Colthup, W. G. Fateley, J. G. Grasselly, The Handbook of Infrared and Raman Characteristic Frequencies of Organic Molecules, Academic Press, San Diego, New York, Boston, London, **1991**.
[23] P. Ropret, T. Kosec, *J. Raman Spectrosc.* **2012**, *43*, 1578.
[24] V. Hayez, T. Segato, A. Hubin, H. Terryn, *J. Raman Spectrosc.* **2006**, *37*, 1211.
[25] C. Chiavari, K. Rahmouni, H. Takenouti, S. Joiret, P. Vermaut, L. Robbiola, *Electrochim. Acta* **2007**, *52*, 7760.
[26] F. Galesse, G. Laguzzi, L. Luvidi, V. Ferrari, S. Takacs, G. Venturi Pagani Cesa, *Corros. Sci.* **2008**, *50*, 954.
[27] L. I. McCann, K. Trentleman, T. Possley, B. Golding, *J. Raman Spectrosc.* **1999**, *30*, 121.